Nature Environment and Pollution Technology
An International Quarterly Scientific Journal

p-ISSN: 0972-6268
(Print copies up to 2016)
e-ISSN: 2395-3454

Vol. 19 | No. 4 | pp.1343-1354 | 2020

Original Research Paper

https://doi.org/10.46488/NEPT.2020.v19i04.001

Open Access Journal

# Realistic Decontamination of $Fe^{2+}$ Ions from Groundwater Using Bentonite/ Chitosan Composite Fixed Bed Column Studies

**M.E.M. Hassouna*† and M. H. Mahmoud****
*Chemistry Department, Faculty of Science, Beni-Suef University 62514, Beni-Suef, Egypt
**Potable Water & Sanitation Company, Beni-Suef, Egypt
†Corresponding author: M.E.M. Hassouna; mhassouna47@hotmail.com; mohamed.hassona@science.bsu.edu.eg

**Nat. Env. & Poll. Tech.**
**Website: www.neptjournal.com**

*Received:* 21-11-2019
*Revised:* 13-12-2019
*Accepted:* 01-03-2020

**Key Words:**
Bentonite
Chitosan
Adsorption
Fixed bed column

## ABSTRACT

Bentonite/chitosan composite was synthesized and characterized by different techniques including XRD, FT-IR, SEM and TEM to detect its physicochemical properties. The composite was introduced in realistic purification application to reduce the dissolved iron content in raw groundwater sample by fixed-bed column system. The plotted breakthrough curves and the related mathematical parameters revealed that the column achieves iron removal percentage of about 69% from 6.6 L of water after adjusting the factors affecting the system at 3 cm bed thickness, 5 mL/min flow rate, 5 mg/L concentration and pH 6. Applying the column system to remove iron from groundwater under the same conditions can achieve iron removal percentage of about 69% from a total volume of 8.2 L of water. The interaction of the metal on the column was attained after 18 hours and the saturation time was attained after 27.5 hours which revealed the high performance of the composite in the designed column system for the purification of groundwater.

## INTRODUCTION

In later periods, the contamination of the water supplies represents the main challenge that faces the modern communities and the contemporary world to provide safe water for populations (Mohamed et al. 2018). One of the commonly recorded water pollutants is the presence of dissolved metal ions that are reported as toxic, non-degradable and having a high tendency to accumulate in the living tissues (Abukhadra et al. 2019a). $Fe^{+2}$ and $Mn^{+2}$ ions are dissolved salts detected extensively in the groundwater wells, especially in the deep ones that are poor in dissolved oxygen.

It was reported that iron ions can be present as dissolved $Fe^{2+}$ or as undissolved species such as $Fe(OH)_3$ (Hassouna et al. 2017, Barloková & Ilavsky 2010). The existence of $Fe^{2+}$ pollutants within the water supplies at high concentrations can reduce the water purity and affect negatively the human health (Ehssan 2012, Al-Anber 2010). Additionally, the common oxidation of $Fe^{2+}$ ions resulted in precipitation of hydroxide suspensions that produce unpleasant colour and taste. Their role in the turbidity of the water supplies was reported (Homoncik et al. 2010). Moreover, the precipitated hydroxide species can cause the generation of some toxic derivatives that commonly resulted in several types of diseases including neoplasia, arthropathy, cardiomyopathy, oliguria, anorexia, neurological disorder and biphasic shock (Sarin et al. 2004, Takeda 2003). The accepted value for the concentrations of $Fe^{2+}$ is recommended not to exceed 0.3 mg/L due to the previous side effects (Abd ElSalam et al.2019). However, the European Union set 0.2 mg/L of iron as the maximum limit in drinking water (European Union 1998).

Biological treatment, oxidation, ion exchange, adsorption and membrane filtrations are the commonly investigated methods in the decontamination of $Fe^{2+}$ (Pathania et al. 2016). Among all the stated technologies, the use of low-cost adsorbents was recommended by numerous researchers as simple and highly effective techniques (Yang et al. 2017, Albadarin et al. 2017). Therefore, several types of natural and synthetic materials were introduced for this target as heulandite, clinoptilolite, bentonite, kaolinite, activated carbon, synthetic zeolite, fly ash, metal oxide and mesoporous silica (Hethnawi et al. 2018, Mohamed et al. 2018).

Bentonite is a common type of clays that can be identified as fine-grained sedimentary rocks and is composed mainly of smectite clay minerals in addition to quartz, and feldspar as associated impurities (Li et al. 2016). It was applied widely as an adsorbent for metal ions as well as other inorganic and organic contaminants. This was attributed to its reported unique properties of flexible chemical and crystalline structure, remarkable surface area, superior adsorption capacities and proved environmental value (Abukhadra et al. 2019 b). Although previous studies were reported about the decon-

tamination of metals by bentonite, numerous studies were conducted to upgrade its adsorption capacities by chemical or physical modification processes (Amadio et al. 2017).

Integration between bentonite and biogenic polymers in hybrid material or composite was investigated as a potential technique to improve the bentonite properties and maximize its uptake capacity (Wang et al. 2016, Jaymand 2014, Bober et al. 2010). Kamińska (2018) has performed efficient removal of organic micro pollutants with different properties from WWTP (wastewater treatment plant) effluent in fixed bed columns packed with several combinations of sand, granular activated carbon (GAC), and granular clay-carbonaceous composite. Two types of bentonite-powder activated carbon-based granules (Ben-AC) were prepared with different calcination temperatures. It was found that higher calcination temperature enhanced the surface porosity and adsorption potential versus studied micro pollutants due to dehydroxylation resulting in higher chemical activity.

Chitosan was studied as one of the best used biogenic polymers that can be integrated with clays in effective and eco-friendly composite (Abukhadra et al. 2019b). Chitosan is a common natural polyaminosaccharide that can be extracted from chitan and has several environmental and technical advantages. It has the advantages of nontoxicity, biocompatibility, biodegradability, bioactivity, high adsorption properties, high physical and mechanical performance (Ngah et al. 2010). Thus, the integration between chitosan and bentonite can be resulted in the development of novel materials of higher adsorption properties than the individual phases (Liu et al. 2014, Tirtom et al. 2012).

Fixed-bed column using chitosan immobilized on bentonite has been used for the removal of copper (Futalan et al. 2011a) and Ni (Futalan et al. 2011b). Chitosan/bentonite/MnO composite beads in fixed-bed operation has been used for manganese removal from water (Muliwa et al. 2018). Adsorption of Pb (II), Cu (II), and Ni (II) from aqueous solution using Chitosan-Coated Bentonite has been performed using fixed bed (Futalan et al. 2012, Tsai et al. 2016). It has been, also, used for the removal of nitrates (Golie et al. 2018). Giannakas & Pissanou (2018) reviewed the use of Chitosan/Bentonite Nanocomposites for wastewater treatment.

Kaolinite nanotubes (KNTs) were synthesized from kaolinite by ultrasonic scrolling (Abukhadra et al. 2019c). KNTs were used as adsorbents for $Zn^{2+}$, $Cd^{2+}$, $Pb^{2+}$, and $Cr^{6+}$ with uptake capacities of 103 mg/g, 116 mg/g, 89 mg/g, and 91 mg/g, respectively.

Arsenic removal has received much attention all over the world because of its toxicity and carcinogenicity (Barakan et al. 2019). As (V) has been adsorbed from aqueous solution onto Fe(III)-impregnated bentonite (Fe-Bent).

Thus, this study aims to introduce realistic treatment and purification of raw groundwater from iron pollutants through fixed bed column based on synthetic bentonite/chitosan composite as low cost and eco-friendly adsorbent. The controlling factors including the pH, bed thickness, flow rate and initial concentrations were studied in details to set the best operating conditions. Moreover, two kinetic models were evaluated to describe the studied system.

## MATERIALS AND METHODS

The used bentonite was collected as representative sample from bentonite quarry, Northern Western Desert, Egypt. Chitosan was delivered as a commercial polymer material by Winlab Company. The used standard iron certified reference (CRM) was obtained from Merck Co. (Germany). Glacial acetic acid (Sigma-Aldrich, 99.8%) was used as dissolvent for chitosan. NaOH pellets and hydrochloric acid solution were used as pH modifiers and were delivered by El-Nasr Company, Egypt for chemical products. The incorporated chemicals in all the experimental tests are of analytical grade and were applied directly without purification.

### Synthesis of Bentonite/Chitosan Composite

The fabrication of the composite has involved the grinding of the raw bentonite by ball mill to fine particles in the size range of 100 μm to 20 μm followed by mechanical mixing with chitosan gel according to (Abukhadra et al. 2019a). This was accomplished by dispersion of 5 g of bentonite powder in about 100 mL of distilled water for 1 h under speed stirring (1000 rpm). Then the bentonite mixture was mixed with chitosan gel that was formed by dissolving 2.5 g of chitosan in about 50 mL of acetic acid (0.1M) and stirred for another 2 h fixing the speed at 1000 rpm. After that, the mixture was treated by ultrasonic waves for (5 h) to accelerate and confirm the intercalation of bentonite sheets by chitosan chains (Fig. 1). Finally, the product was separated and dried at 60°C for 10 h and kept for further characterization and application.

### Characterization Techniques

The crystalline properties were studied based on the obtained X-ray diffraction patterns of bentonite, chitosan and bentonite/chitosan composite using X-ray diffractometer [PANalytical (Empyrean)]. External morphological properties and the internal structure after the intercalation process were studied using Scanning-Electron Microscope (Gemini, Zeiss-Ultra 55) and Transmission-Electron Microscope (JEOL-JEM2100). The change in the active functional groups before and after the intercalation process was inspected by Bruker spectrometer FT-IR (Vertex 70).

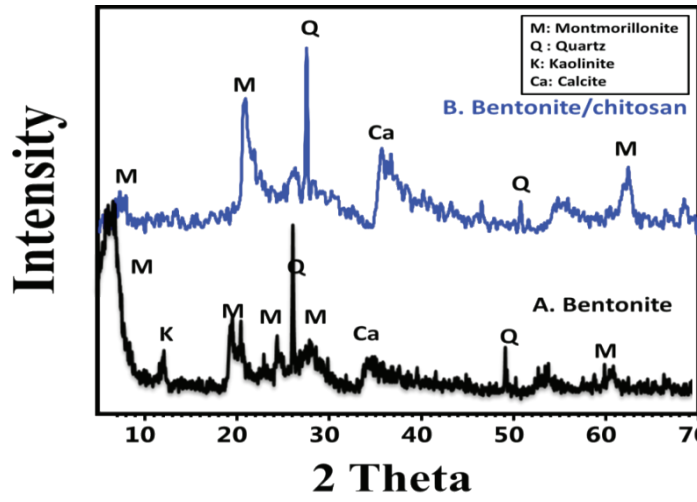


Fig. 1: XRD patterns of bentonite (A) and bentonite/chitosan composite (C).

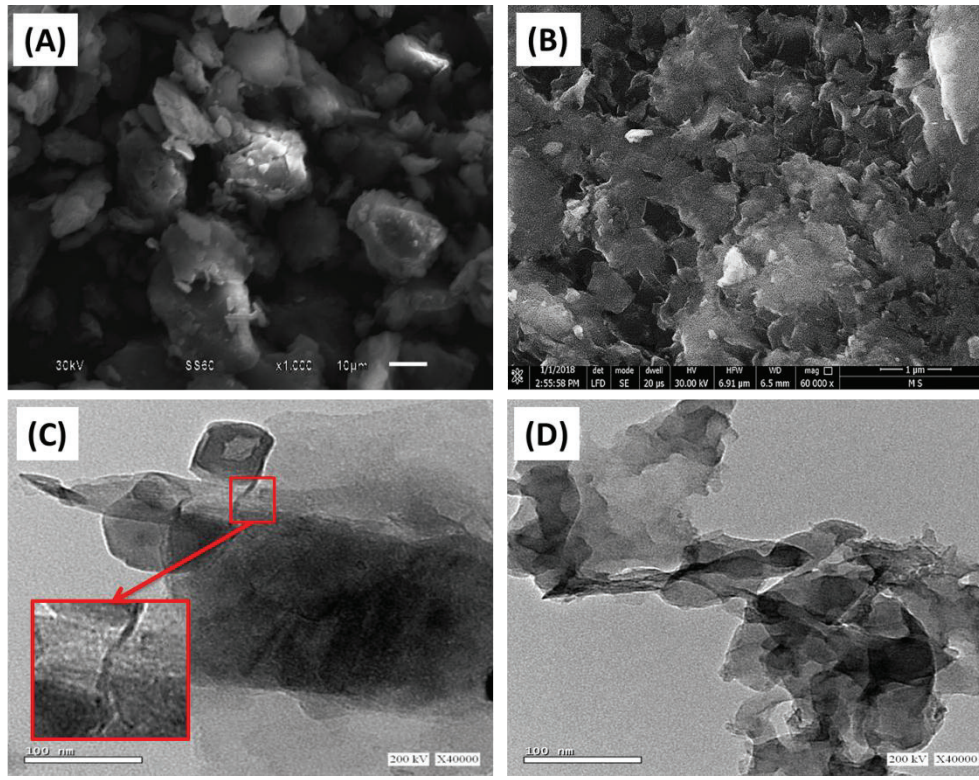


Fig. 2: SEM images of bentonite (A) and bentonite/chitosan composite (B); and the TEM images (C) and (D).

The residual iron concentrations after the test were estimated using inductively coupled plasma mass spectrometer (ICP-MS; Perkin Elmer) with detection limit of about 0.1 mg/L. The reference solutions which were used match the requirements of CRM standard iron of the National institute of standard and technology. The measured results are the average values obtained after triplicate tests with a standard deviation lower than 6 %.

### Adsorption Tests

**Collecting the raw water samples:** The groundwater samples were collected from different groundwater wells in Beni-Suef Governorate, Middle Egypt. The samples were set in polypropylene containers that were washed using dilute nitric acid and then rinsed using distilled water. Then, water samples were acidified by nitric acid to reduce the pH value to be less than 2 as critical step to avoid the possible adsorption of $Fe^{2+}$ on the polypropylene walls of the used containers (APHA 1999). Then the preserved samples were kept in a refrigerator at about 4°C to avoid the predicted evaporation at room temperature.

### Fixed Bed Column Study

**Designing the column system:** The used column system was composed of glass cylinder with 2 cm internal diameter and 15 cm length ending with an outlet leading to a pump (Fig. 4). The bentonite/chitosan bed was packed and inserted in the glass between two separated layers of polyethylene wool supported by plastic mesh to avoid the leaching of the adsorbent particles.

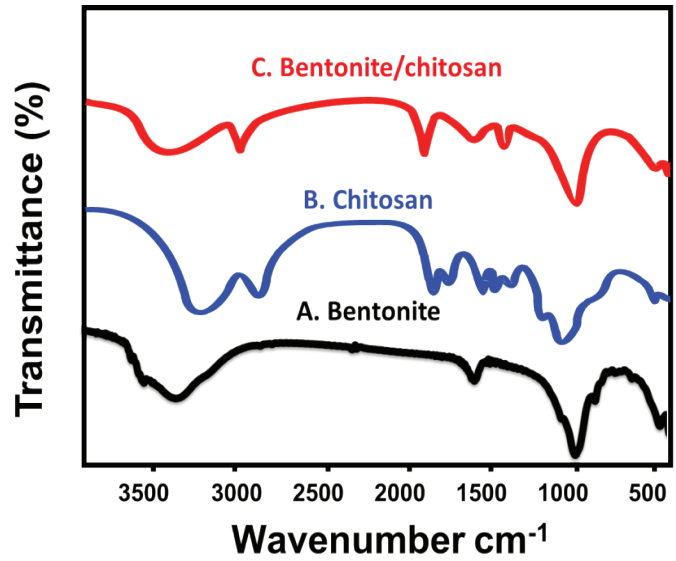


Fig. 3: FT-IR spectra of bentonite (A), chitosan (B) and bentonite/chitosan composite (C).

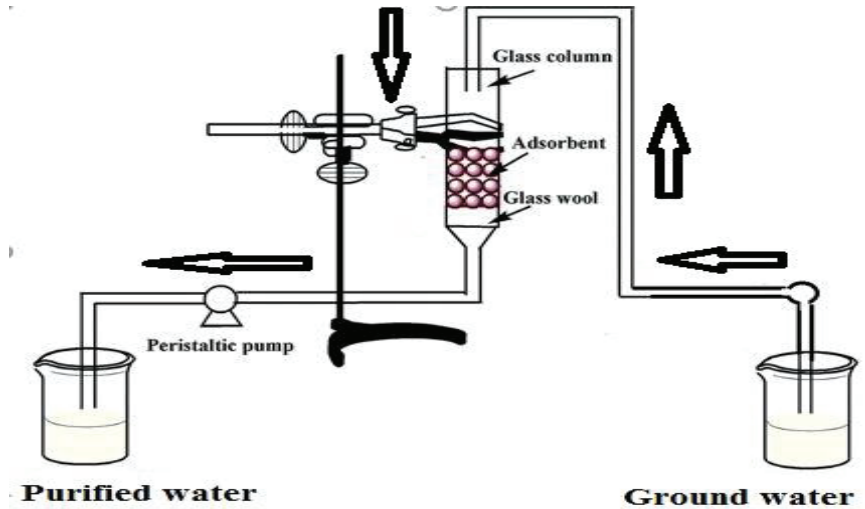


Fig. 4: Fixed-bed column.

Water samples were pumped through the column and after regular intervals of (60 min), the filtrated waters were collected to measure the residual metal concentrations. The controlling factors were studied considering pH within a range from (3 to 7), and the other factors were adjusted at 0.02 g of bentonite/chitosan mass, 100 mL solution volume, time of 120 min and 10 mg/L concentration. The bed height (thickness) was studied within a range from 1-3 cm after fixing the other conditions at 10 mg/L concentration, 5 mL/min flow rate and 1440 min total filtration time. Also, the influence of flow rate was studied within a range from 5 mL/min to 15 mL/min at fixed values of 3 cm bed thickness, 10 mg/L concentration and 24 hours total time. Finally, the effect of concentration was studied within a range from 5 mg/L to 15 mg/L at fixed values of 3 cm thickness, 5 mL/min flow rate and 24 hours total filtration time.

**Fixed bed column data analysis:** The performance of bentonite/chitosan-based column system was checked according to the theoretical parameters of the plotted curves for residual concentration ($C_{eff}$)/ initial concentration ($C_o$) versus the filtration time. The breakthrough points and exhausted points of the curves were estimated at $C_{eff}$ of about 10 % and $C_o$ of about 95 %, respectively. The obtained volumes of the effluents ($V_{eff}$ (mL)) were measured from Eq.(1) (Zhang et al. 2015):

$$V_{eff} = Q\ x\ t_{total} \quad \ldots(1)$$

Where Q denotes the volumetric flow rate in mL/min and $t_{total}$ is the flow time. All the mathematical parameters of the system were estimated according to the linear equations from Eq.(2) to Eq.(6) (Abukhadra et al. 2019b).

$$C_{ad} = C_o - C_{eff} \quad \ldots(2)$$

$$q_{total}(mg) = \frac{QA}{1000} = \frac{Q}{1000}\int_{t=0}^{t=t_{total}} C_{ad}\, dt \quad \ldots(3)$$

$$M_{total}(mg) = \frac{CQt_{total}}{1000} \quad \ldots(4)$$

$$q_{eq}(mg/g) = \frac{q_{total}}{X} \quad \ldots(5)$$

$$Total\ removal\ .,\%\ (R.,\%) = \frac{q_{total}}{M_{total}}\ 100 \quad \ldots(6)$$

Where the symbols denote the adsorbed ions ($C_{ad}$), total adsorbed ions ($q_{total}$), the area of the plotted breakthrough curves (A), the total pumped ions in the system ($M_{total}$), the uptake equilibration ($q_{eq}$) and the used bentonite/chitosan mass (X).

## RESULTS AND DISCUSSION

### Characterization

**Structural properties:** The structural and crystalline properties of bentonite and bentonite/chitosan composite were inspected based on the obtained XRD pattern (Fig.1). The used raw sample of bentonite showed XRD pattern with characteristic peaks of montmorillonite as the main clay mineral of the smectite group and as the dominant component of the sample in addition to other crystalline phases of kaolinite, calcite and quartz minerals that can be identified as impurities. Montmorillonite minerals were detected with their identification peaks at different temperatures as 6.54°C, 19.84°C, 25°C and 28.34°C, respectively that are related to the lattice planes of (002), (020) and (105), respectively (card No: 00-003-0010).

The intercalation of chitosan chains between bentonite layers was reflected in the resulted XRD pattern as the peaks that were deviated from their normal positions and the main peak was detected at 6.3° with low diffraction intensity. The recorded increase in the d-spacing to 13.91Å for bentonite/chitosan composite as compared to 13.486Å for raw bentonite revealed successful fabrication of the bentonite/chitosan composite by intercalation process.

**Morphological properties:** The morphological properties of bentonite and bentonite/chitosan composite were studied using SEM and TEM images. The SEM images reflected the presences of bentonite as compacted sheets of montmorillonite and decorated by tiny nudes related to the associated mineral impurities (Fig. 2A). The intercalation of montmorillonite sheets by chitosan revealed considerable changes in the surface morphology of bentonite. The surface of the composite exhibits a network structure of noticeable interstitial microspores in addition to irregular fibrous particles related mainly to the admixed chitosan (Fig. 2B). The integration between bentonite and chitosan also was confirmed by TEM images (Fig. 3). The studied bentonite particles are of multi-layered structure and showed characteristic lattice fingers (Fig. 3B). After the integration between it and chitosan chains, the composite appeared as hybrid material composed of bentonite sheets and fibrous particles of chitosan (Fig. 3C).

However, several studies revealed the reduction in the specific area after the modification of bentonite by chitosan, the synthetic composite in the introduced study declared slight enhancement in it as it increased from 91 $m^2/g$ for raw bentonite to 98.44 $m^2/g$ for bentonite/chitosan composite, respectively. This can be explained by the reported formation of bentonite/chitosan composite as an interlocked network structure forming a secondary porous matrix.

**Chemical functional groups:** The changes in the chemical functional groups were monitored based on the FT-IR spectra of bentonite and bentonite/chitosan composite, the main groups are displayed in Table 1. The main chemical groups of

clay minerals were identified in the bentonite sample as OH, Si-O-Si, and Al-O (Table 1). Also, chitosan as single-phase was identified by its characteristic amide, aliphatic C-H, N-H, and C-O groups. The integration between the bentonite layers and chitosan chains also was reflected in the FT-IR results. The obtained bands revealed the formation of hybrid material of heterogeneous functional groups related to both bentonite and chitosan (Table 1). Additionally the appearance of such mixed bands associated with clear deviation from their normal positions confirming the successful intercalation of bentonite layer by chitosan (Fig. 3 and Table 1).

## Fixed Bed Column Studies

The initial pH plays a vital role in controlling the surface properties of the adsorbent as well as the speciation of the dissolved metals (Seliem et al. 2016, Ozdes et al. 2009). The influence of pH on the uptake properties of bentonite chitosan for $Fe^{2+}$ ions was studied within the pH range from 2 to 7 to avoid the possible precipitation of iron at the high alkaline conditions (Ehssan 2012). The experimental results declared continuous enhancement in the removal percentages of iron with the regular expanding in the pH value achieving the best results at the highest pH 7. The removal percentages were augmented by 26 %, 40 %, 64 %, 78 % and 80 % with the increment of pH.

This makes it a promising material for realistic purification of polluted water resources. The previous behaviour can be elucidated based on the proton-competitive adsorption phenomenon at the different studied pH conditions. The regular increase in the value of pH associated with a noticeable reduction in the concentration of the present hydronium ions that act as competitors with adsorbed metal ions and in turn promotes the uptake of $Fe^{2+}$ ions by bentonite/chitosan composite (Sprynskyy et al. 2006). Moreover, the alkaline conditions can accelerate the dissociation of the counter ions within the clay matrix which can reduce the uptake capacities (Hassouna et al. 2014). Fig. 4 shows a detailed diagram for the fixed bed column.

## Effect of Bed Thickness

The obtained breakthrough curves with the different thicknesses of the bentonite/chitosan bed are illustrated in Fig. 5B. Generally, the column performance shows noticeable enhancing with the regular increment in the bed thickness. The obtained breakthrough time ($t_b$) for the treated solutions was enhanced by 27, 37.5 and 42.5 hours with the regular increment in the bentonite/chitosan bed thickness by 1, 2 and 3 cm, respectively. Also, this was reflected in the obvious increment in the required time till saturation or the exhausting of the column to be 45, 52.5 and 55 hours, for the same thickness in order (Table 1). The previous observations reflected the possible enhancing in the lifetime and the operation of bentonite/chitosan-based column with the regular increase in its thickness of the bed as well as the treated water volumes.

The quantities of the adsorbed $Fe^{2+}$ ions by bentonite/chitosan bed of 1, 2 and 3 cm thicknesses were 592, 737 and 947 mg, respectively, which was reflected in the total removal percentage of iron ions. The resulted total removal percentages by the end of the filtration time were 40.8 %, 50.75 % and 65.2% corresponding to bentonite/chitosan beds with thicknesses of 1, 2 and 3 cm, respectively. This was related to the role of the high bed thickness in reducing the axial dispersions of mass transfer and in turn, promote the diffusion of $Fe^{2+}$ ions onto the synthetic bentonite/chitosan

Table 1: FT-IR spectral bands and the related functional groups of bentonite, chitosan, and bentonite/chitosan composite.

| Band Positions ($cm^{-1}$) | | | Chemical functional group |
|---|---|---|---|
| BE | CH | BE/CH | |
| 3480 | - | 3494 | Attributed to the OH group of the crystal structure and water absorbed by bentonite (Abukhadra et al. 2019) |
| - | 3387.5 | - | Overlap between OH and N-H (Zhu et al. 2009) |
| - | 2911 | 2916.3 | Stretching of aliphatic C-H (Zhu et al. 2009) |
| - | 1653 | 1651.4 | Bending of N-H group (Liu et al. 2015) |
| 1640.6 | - | 1644.5 | Water within the interlayers |
| - | 1452 | 1455 | Bending of N-H group (Abukhadra et al. 2019) |
| - | 1373 | - | Bending of C-H group (Abukhadra et al. 2019) |
| - | 1084 | - | Stretching of C-O group (Liu et al. 2015) |
| 1000 | - | 1022.4 | Si-O group (Hassouna et al. 2017) |
| 918 | - | - | Al-O groups (Abukhadra et al. 2018) |
| 400-1000 | - | 400-100 | Mg-$Fe^{2+}$-OH, Si-O-Al and Si-O-Mg groups (Abukhadra et al. 2018) |

composite as an adsorbent (Mohan et al. 2017). Therefore, the pumped polluted solutions spent high time intervals in close contact with the bentonite/chitosan composite. Also, using high bed thickness increases the number of active uptake sites which increase the quantities of captures of iron ions.

**Determination of Adsorption Isotherm Parameters**

At room temperature, the required quantity (in gram) of the investigated adsorbent is added to a 1 L of the contaminated water sample.

The adsorption was performed with constant stirring of the reaction medium using jar test Phipps bride stirrer (Model 7790-402, USA). After a certain time, the solution with dispersed adsorbent was filtered. The experiment was carried out using different doses of the adsorbent (10-1000 ppm) for different time intervals. An aliquot of 10 mL was taken for the ICP measurements. Adsorption isotherm of the investigated metal ions ($Fe^{+2}$) by the prepared column was determined over a wide range of metal ion concentrations. The adsorption isotherm curves and adsorption parameters were calculated using Langmuir and Freundlich models (Dada et al. 2012).

$$q_e = \frac{Q_m\, bC_e}{1+ C_e}$$ Non-linear form $$\frac{C_e}{q_e} = \frac{C_e}{Q_m} + \frac{1}{Q_m\, b}$$ linear form

Both $Q_m$ and b are calculated from the slope and intercept of the linear relationship between $C_e/q_e$ and $C_e$ respectively.

Freundlich adsorption model is $q_e = Kf\, C_e 1/n$ nonlinear form but the linear form is

$$\log q_e = \log Kf + (1/n) \log C_e.$$

Both Kf and n are calculated from the intercept and slope of the linear relationship of double logarithmic of $q_e$ and $C_e$.

Where, $q_e$ is the equilibrium concentration of adsorbed metal ion on polymer surface (mg/g). $C_e$ is the bulk concentration of metal ion at equilibrium (mg/L). $Q_m$ is the monolayer adsorption capacity (mg/g), b is a constant related to the adsorption equilibrium constant and Kf & n are dimensionless constants refer to the adsorption capacity and adsorption intensity respectively.

**Adsorption isotherms**: The effect of metal ion concentrations on the removal efficiency of the investigated polymeric sample was studied. The quantity of the polymers was kept constant at 50 ppm at room temperature. Both, the Langmuir model which describes the monolayer adsorbate on

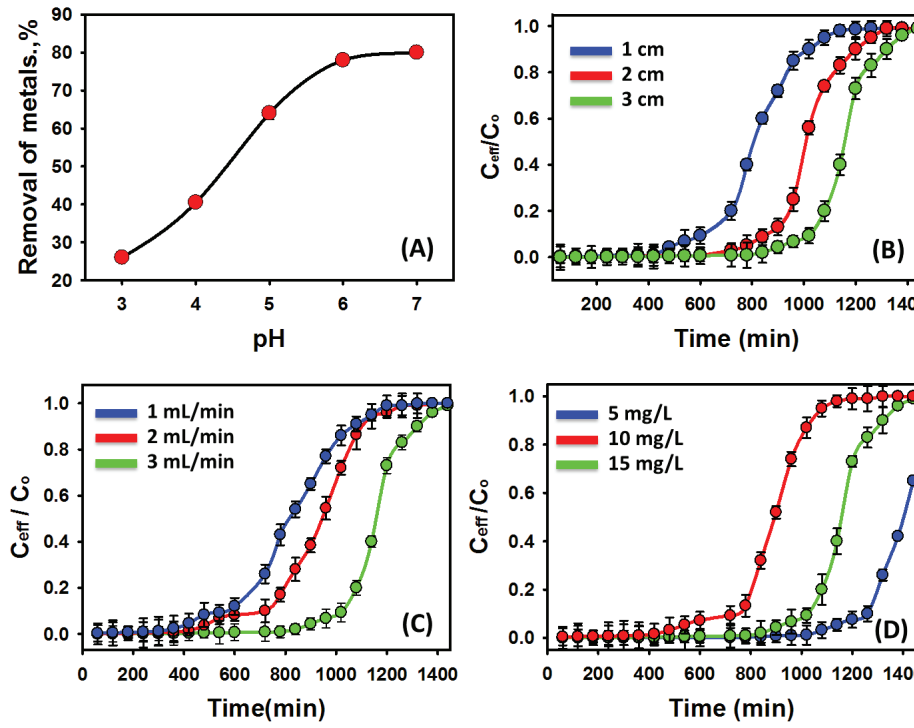


Fig. 5: Effect of solution pH on the removal of iron from water (A), removal of iron at different bed thickness (B), at different operating flow rates (C) and at different initial bentonite/chitosan concentrations (D).

the surface of the adsorbent and Freundlich model which describes the multilayer adsorptions have been investigated. The linear relationships of both isotherm models are graphically presented in Figs. 6 and 7, from which the Langmuir and Freundlich isotherm parameters were calculated and given in Table 3.

**Effect of Flow Rate**

The performance of bentonite/chitosan-based column system using different flow rates for the studied iron polluted solutions was presented graphically in Fig.5C and the related theoretical parameters are listed in Table 1. The performance of the system was largely affected by increasing the solution flow rate, as the time was decreased by 42.5, 30 and 25 hours by expanding the flow rate by 5, 10 and 15 mL/min, respectively. Additionally, the saturation time or the column exhaustion interval was reduced significantly by 57, 50 and 47.5 hours for the same studied flow rates in the order which will reduce the lifetime of the system.

However, on increasing the flow rates of the pumped solution associated with an observable increment in the total purified volumes, there was a noticeable reduction in the total removal percentage of $Fe^{2+}$ ions, upon which 5 mL/min was set as the best flow rate for the bentonite/chitosan fixed-bed column system (Table 2). The reported results for the influence of higher flow rates in reducing the residence time between the composite bed and iron polluted solution have affected negatively the required contact time for promising uptake of dissolved $Fe^{2+}$ ions (Nazaria et al. 2016). The slower flow rates provide long residence times for effective diffusion of $Fe^{2+}$ ions between the composite grains which increase the uptake chances by more active adsorption sites (Abdolali et al. 2017).

**Effect of Initial Concentration**

The influence of iron concentrations on the studied bentonite/chitosan-based column system was investigated using three different concentrations (5, 10, 15 mg/L). The results were plotted in breakthrough curves (Fig. 5D) and the related theoretical parameters were estimated and listed in Table 1. The plotted curves emphasized the obvious reduction in breakthrough as well as the saturation time with the increment in $Fe^{2+}$ concentration from 5 mg/L to 15 mg/L. Such behaviour was explained by several authors to be a result of the large concentration gradient and the low mass transfer resistance that is associated with using high concentrations of the inspected pollutants in addition to the expected saturation of the composite adsorption sites by the adsorbed $Fe^{2+}$ ions (Abdolali et al. 2017). Therefore, the performance of the column and its lifetime affected negatively the over increase in the concentrations of the dissolved water pollutants.

**Purification of Raw Groundwater Samples**

The purification of real groundwater sample was performed after adjusting the controlling factors at 3 cm for the bentonite/chitosan composite bed thickness, 5mL/min as flow rate and pH 7 for total filtration time of 7 hours. The chemical analysis of the studied real groundwater sample

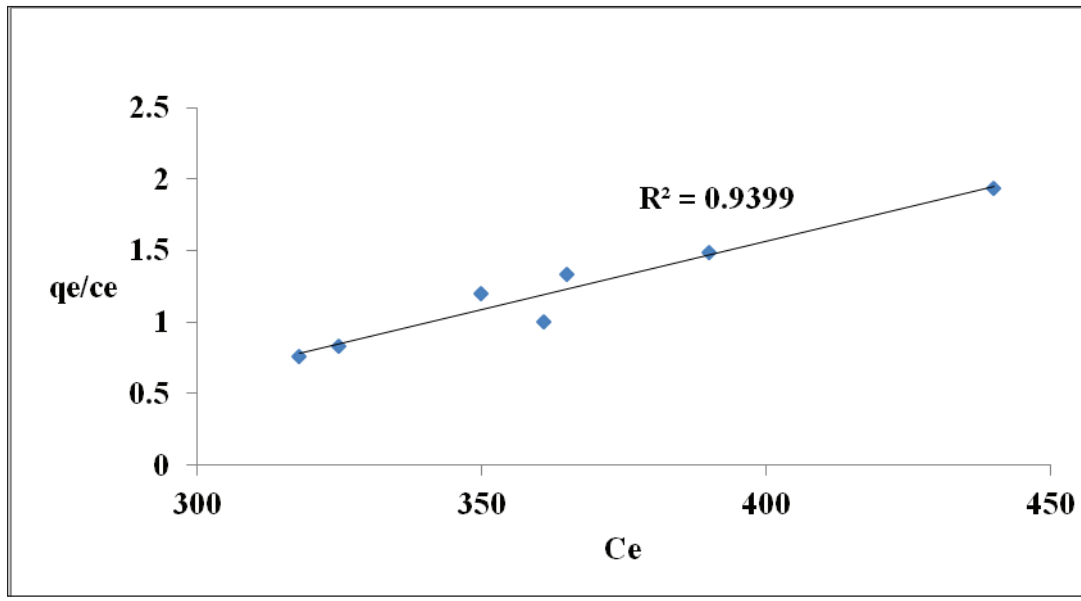


Fig. 6: Langmuir isotherm plot of iron adsorption.

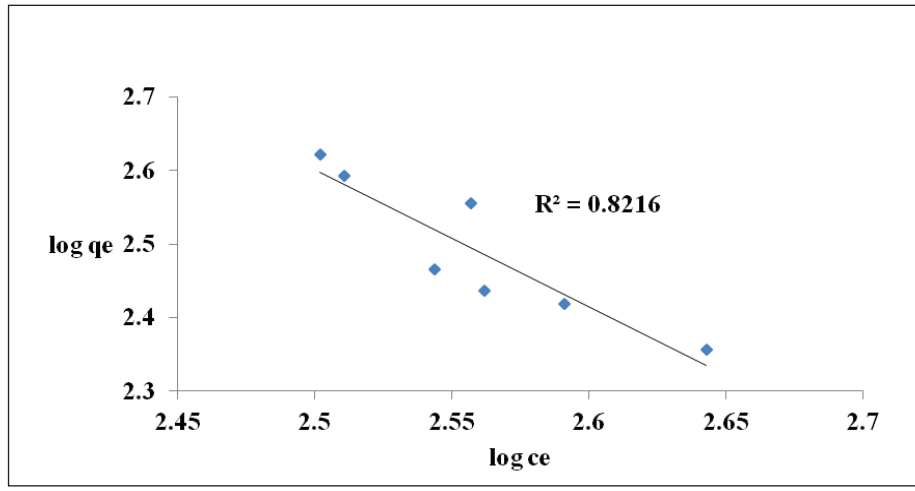


Fig. 7: Freundlich isotherm plot of iron adsorption

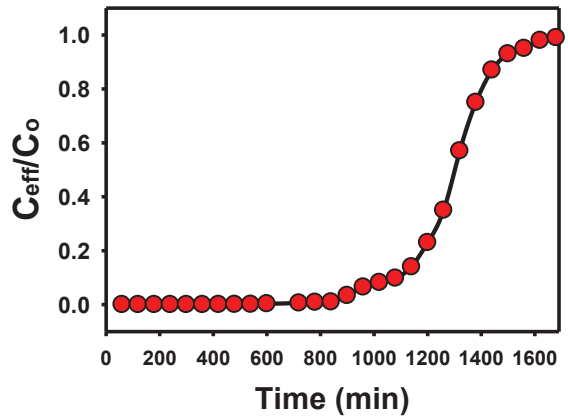


Fig. 8: The removal of iron from raw groundwater samples.

Table 2: Mathematical parameters of bentonite/chitosan continuous fixed-bed column system.

| Bed height | Flow rate | Conc. | $C_{ad}$ (mg/L) | q ($_{total}$) mg | $q_{eq}$ (mg/) | M $_{(total)}$ Mg | R. (%) | $t_b$ (min) | $t_s$ (min) | $V_{eff}$ (mL) |
|---|---|---|---|---|---|---|---|---|---|---|
| Aqueous solutions | | | | | | | | | | |
| 1cm | 5mL/min | 10 mg/L | 318 | 592 | 418 | 1452 | 40.8 | 650 | 1080 | 5400 |
| 2cm | 5mL/min | 10 mg/L | 350 | 737 | 292 | 1452 | 50.75 | 900 | 1260 | 6000 |
| 3cm | 5mL/min | 10 mg/L | 390 | 947 | 263 | 1452 | 65.2 | 1020 | 1380 | 6300 |
| 3cm | 10mL/min | 10 mg/L | 325 | 1516 | 391 | 2904 | 52.2 | 720 | 1200 | 11400 |
| 3cm | 15mL/min | 10 mg/L | 361 | 1376 | 360 | 4356 | 31.6 | 600 | 1140 | 15300 |
| 3cm | 5mL/min | 5mg/L | 365 | 982 | 273 | 1089 | 90.2 | 1260 | --- | 6600 |
| 3cm | 5mL/min | 15 mg/L | 440 | 778 | 227 | 2541 | 30.6 | 720 | 1080 | 5100 |
| Raw groundwater | | | | | | | | | | |
| The sample | | | 85 | 112.5 | 70.4 | 163 | 69 | 1080 | 1560 | 8200 |

Table 3: Langmuir and Freundlich isotherm parameters.

| Ce | qe | Ln ce | Ln qe | ce/qe | log ce | log Qe |
|---|---|---|---|---|---|---|
| 318 | 418 | 5.76 | 6.03 | 0.760766 | 2.502 | 2.621 |
| 350 | 292 | 5.85 | 6.83 | 1.19863 | 2.544 | 2.465 |
| 390 | 263 | 5.96 | 5.57 | 1.48289 | 2.591 | 2.419 |
| 325 | 391 | 5.78 | 5.96 | 0.831202 | 2.511 | 2.592 |
| 361 | 360 | 5.88 | 5.88 | 1.002778 | 2.557 | 2.556 |
| 365 | 273 | 5.89 | 5.60 | 1.336996 | 2.562 | 2.436 |
| 440 | 227 | 6.08 | 5.42 | 1.938326 | 2.643 | 2.356 |

Table 4: The chemical composition of the studied raw groundwater.

| Parameters | Sample value |
|---|---|
| Turbidity (NTU) | 45 |
| pH | 7.49 |
| Alkalinity (mg/L ) | 189 |
| Conductivity (Us/cm) | 1315 |
| Total hardness (mg/L) | 191 |
| Ca hardness (mg/L) | 112 |
| Mg hardness (mg/L) | 79 |
| Chloride (mg/L) | 103 |
| Sulfate (mg/L) | 150 |
| Ammonia (mg/L) | 0.62 |
| Nitrite (mg/L) | 0.009 |
| Nitrate (mg/L) | 7.05 |
| Iron (mg/L) | 0.4 |
| Manganese (mg/L) | 0.91 |
| Cu (mg/L) | 0.009 |
| Zn (mg/L) | 0.02 |

showed the presence of different types of dissolved contaminants (Table 4). The iron content was 0.4 mg/L which exceeds the accepted limit; this also was recorded for the contents of manganese and ammonia which can affect the adsorption trend of iron in the system (Table 2). The resulted curve for fixed-bed purification of the groundwater sample from dissolved iron appears in Fig. 8 and the performance mathematical parameters are presented in Table 1.

The breakthrough time and saturation time were attained after 45 and 65 hours, respectively. The detected reduction in the obtained breakthrough time as well as the saturation time for groundwater as compared to the prepared aqueous solution of 5 mg/L concentration related the existence of other dissolved elements and compounds that affect the affinity of bentonite/chitosan composite for the dissolved iron. The results reflected that the column has capacity to adsorb about 112 mg as total adsorbed iron and the equilibrium capacity is 70 mg/g. This was associated with total removal percentage of about 69% for the total treated volume of 8200 mL.

## CONCLUSION

Bentonite/chitosan composite was synthesized as an adsorbent for iron ions from water. Its adsorption properties were studied by continuous fixed-bed column system. The mathematical parameters of the breakthrough curves showed removal percentage of about 90% from 6.6 L of the aqueous solution after adjusting the factors of the system at 3 cm bed thickness, 5 mL/min flow rate, 5 mg/L concentration and at pH 6. For the groundwater at the same conditions, iron removal percentage reached 69% for 8.2 L of treated water. The breakthrough and the saturation times were attained after 45 and 68.5 hours, respectively.

## REFERENCES

Abukhadra, M.R., Dardir, F.M., Ahmed, E.A. and Soliman, M.F. 2019a. Efficient removal of Sr ions from water utilizing a novel Ni/$Fe^{+2}$-doped spongy apatite through fixed-bed column system: optimization and realistic application. Clean Technologies and Environmental Policy, 21: 69-80. doi.org/10.1007/s10098-018-1616-1.

Abukhadra, M.F., Adlii, A. and Bakry, B.M. 2019b. Green fabrication of bentonite/chitosan cobalt oxide composite (BE/CHCo) of enhanced adsorption and advanced oxidation removal of Congo red dye and Cr(VI) from water. International Journal of Biological Macromolecules, 126: 402-413. doi.org/10.1016/j.ijbiomac.2018.12.225.

Abukhadra, M.R., Bakry, B.M., Adlii, A., Yakout, S.M. and El-Zaidy, M.E. 2019c. Facile conversion of kaolinite into clay nanotubes (KNTs) of enhanced adsorption properties for toxic heavy metals ($Zn^{2+}$, $Cd^{2+}$, $Pb^{2+}$ and $Cr^{6+}$) from water. J. Hazard. Mater., 374: 296-308. doi: 10.1016/j.jhazmat.2019.04.047.

Abukhadra, M.R., Shaban, M., Sayed, F. and Saad, I. 2018. Efficient photocatalytic removal of safarnin-O dye pollutants from water under sunlight using synthetic bentonite/polyaniline $Ni_2O_3$ photocatalyst of enhanced properties. Environmental Science and Pollution Research, 25(33): 33264-33276. doi.org/10.1007/s11356-018-3270-x.

Albadarin, A.B., Collins, M.N., Naushad, M., Shirazian, S., Walker, G. and Mangwandi, C. 2017. Activated lignin-chitosan extruded blends for efficient adsorption of methylene Blue. Chemical Engineering Journal, 307: 264-272. doi.org/10.1016/j.cej.2016.08.089.

Abd ElSalam, H.M., Kamal, E.H.M. and Ibrahim, M. S. 2018. Cleaning of wastewater from total coliform using chitosan-grafted-poly (2-methy-

laniline). Journal of Polymers and the Environment, 26(8): 3412-3421. https://doi.org/10.1007/s10924-018-1225-4.

Abdolali, A., Ngo, H.H., Guo, W., Zhou, J.L., Zhang, J., Liang, S., Chang, S.W., Nguyen, D.D. and Liu, Y. 2017. Application of a breakthrough biosorbent for removing heavy metals from synthetic and real wastewaters in a lab-scale continuous fixed-bed column. Biores. Technol., 229: 78-87. doi: 10.1016/j.biortech.2017.01.016.

Al-Anber, M.A. 2010. Removal of high-level $Fe^{3+}$ from aqueous solution using natural inorganic materials: Bentonite (NB) and quartz (NQ). Desalination, 250(3): 885-891. doi:10.1016/j.desal.2009.06.071.

Amadio, T. M., Hotza, D., Neto, J.B.R., Blosi, M., Costa, A.L. and Dondi, M. 2017. Bentonites functionalized by impregnation with $TiO_2$, Ag, Pd and Au nanoparticles. Applied Clay Science, 146: 1-6.

APHA 1999. Standard Methods for the Examination of Water and Wastewater, Amer Public Health Assn; 20th edition.

Barakan, S., Aghazadeh, V., Samiee, A. and Mohammadi, S. 2019. Thermodynamic, kinetic and equilibrium isotherm studies of As(V) adsorption by Fe(III)-impregnated bentonite. Environment Development and Sustainability, 10.1007/s10668-019-00424-2.

Barloková, D. and Ilavský, J. 2010. Removal of iron and manganese from water using filtration by natural materials of disposers. J. Environ. Stud., 19(6): 1117-1122.

Bober, P., Stejskal, J., Spírková, M., Trchová, M., Varga, M. and Proke, J. 2010. Conducting polyaniline-montmorillonite composites. Synthetic Metals, 160: 2596-2604.

Dada, A.O, Olalekan, A.P., Olatunya, A.M. and Dada, O. 2012. Langmuir, Freundlich, Temkin and Dubinin-Radushkevich isotherms studies of equilibrium sorption of $Zn^{2+}$ unto phosphoric acid modified rice husk. IOSR Journal of Applied Chemistry (IOSR-JAC), 3(1): 38-45. http://dx.doi.org/10.9790/5736-0313845.

Ehssan, M.N. 2012. Utilization of bentonite as an adsorbent material in the removal of iron. Int. J. Eng. Sci. Technol., 4: 4480-4489.

European Union 1998. Richtlinie 98/83/EG des Rates.

Futalan, C., Kan, C., Dalida, M.L. and Pascua, C. 2011a. Fixed-bed column studies on the removal of copper using chitosan immobilized on bentonite. Carbohydrate Polymers, **83**(2): 697-704. DOI: 10.1016/j.carbpol.2010.08.043.

Futalan, C.M., Kan, C.C., Dalida, M.L.P, Pascua, C., Hsien, K.J. and Wan, M.W. 2011b. Nickel removal from aqueous solution in fixed bed using chitosan-coated Bentonite. Sustain. Environ. Res., 21(6): 361-367.

Futalan, C.M., Tsai, W.C., Lin, S.S., Dalida, M.L. and Wan, M.W. 2012. Copper, nikel and lead adsorption from aqueous solution using chitosan-immobilized on bentonite in ternary system. Sustain. Environ. Res., 22: 345-355.

Giannakas, A. and Pissanou, M. 2018. Chitosan/bentonite nanocomposites for wastewater treatment: a review. SF J. Nanochem. Nanotechnol., 1(1): 1010-1021.

Golie, W.M., Ambethkar, Y. and U. Sreedevi, U. 2018. Recovery of nitrate from water using chitosan/bentonite biocomposite in a continuous stirred tank reactor. J. Environ. Bio. Res., 2(1): 1-3.

Hassouna, M.E.M., Shaban, M. and Nassif, F.M. 2017. Adsorptive removal of iron and manganese from groundwater using CNTs clay and organo-clay nano composites. International Journal of Chemistry and Aquatic Sciences (IJCA), 3(1): 1-21.

Hassouna, M.E.M., Shaban, M. and Nassif, F.M. 2014. Removal of iron and manganese ions from ground water using kaolin sub micro powder and its modified forms. Int. J. Bioassays, 3(07): 3137-3145. DOI:10.21746/ijbio.2014.07.006.

Hethnawi, A., Manasrah, D. A., Vitale, G. and Nassar, N.N. 2018. Fixed-bed column studies of total organic carbon removal from industrial wastewater by use of diatomite decorated with polyethylenimine functionalized pyroxene nanoparticles. Journal of Colloid and Interface, 513: 28-42. DOI: 10.1016/j.jcis.2017.10.078.

Homoncik, S.C., MacDonald, A.M., Heal, K.V., Dochartaigh, B.E.O. and Ngwenya, B.T. 2010. Manganese concentrations in Scottish groundwater. Sci. Total Environ., 408: 2467-2473. doi: 10.1016/j.scitotenv.2010.02.017.

Jaymand, M. 2014. Conductive polymers/zeolite (nano-) composites: under-exploited materials. RSC Adv., 4: 33935-33954. doi: 10.1039/C4RA03067B.

Kamińska, G. 2018. Removal of organic micropollutants by grainy bentonite-activated carbon adsorbent in a fixed bed column. Water, 10(12): 1791-1804. doi:10.3390/w10121791.

Kumar, M. and Puri1, A. 2012. A review of permissible limits of drinking water. Indian J. Occup. Environ. Med., 16(1): 40-44. doi: 10.4103/0019-5278.99696.

Li, N., Yang, B., Xu, L., Xu, G., Sun, W. and Yu, S. 2016. Simple synthesis of $Cu_2O$/Na-bentonite composites and their excellent photocatalytic properties in treating methyl orange solution. Ceramics International, 42(5): 5979-5984. doi: 10.1016/j.ceramint.2015.12.145.

Liu, Q., Yang, B., Lujie, Z. and Huang, R. 2014. Adsorption of an anionic azo dye by cross-linked chitosan/bentonite composite. International Journal of Biological Macromolecules, 72: 1129-1135. doi: 10.1016/j.ijbiomac.2014.10.008.

Mohamed, F. M.R., Abukhadra, M.R. and Shaban, M. 2018. Removal of safranin dye from water using polypyrrole nanofiber/Zn-$Fe^{+2}$ layered double hydroxide nanocomposite (Ppy NF/Zn-$Fe^{+2}$ LDH) of enhanced adsorption and photocatalytic properties. Science of the Total Environment, (640-641): 352-363. https://doi.org/10.1016/j.scitotenv.2018.05.316.

Mohan, S., Singh, D.K., Kumar, V. and Hasan, S.H. 2017. Effective removal of fluoride ions by rGO/$ZrO_2$ nanocomposite from aqueous solution: fixed bed column adsorption modelling and its adsorption mechanism. J. Fluor. Chem., 194: 40-5.

Muliwa, A., Leswifi, T.Y., Maity, A., Ochieng, A. and Onyango, M. 2018. Fixed-bed operation for manganese removal from water using chitosan/bentonite/MnO composite beads. Environmental Science and Pollution Research, 25(4). doi: 10.1007/s11356-018-1993-3.

Nazaria, G., Abolghasemi, H., Esmaieli, M. and Pouya, E.S. 2016. Aqueous phase adsorption of cephalexin by walnut shell-based activated carbon: a fixed-bed column study. Appl. Surf. Sci., 375: 144-153. doi.org/10.1016/j.apsusc.2016.03.096.

Ngaha, W.S.W., Teonga, L.C. and Hanafiah, M.A.K.M. 2011. Adsorption of dyes and heavy metal ions by chitosan composites. Carbohydrate Polymers, 83: 1446-1456. doi:10.1016/j.carbpol.2010.11.004.

Ozdes, D., Gundogdu, A., Kemer, B., Duran, C., Senturk, H.B. and Soylak, M. 2009. Removal of Pb (II) ions from aqueous solution by a waste mud from copper mine industry: equilibrium, kinetic and thermodynamic study. J. Hazard. Mater., 166: 1480-1487. doi: 10.1080/19443994.2012.669161.

Pathania, D., Gupta, D., Al-Muhtaseb, A.H., Sharma, G., Kumar, A., Naushad, M., Ahamad, T. and Alshehri, S.M. 2016. Photocatalytic degradation of highly toxic dyes using chitosan-g-poly(acrylamide)/ZnS in presence of solar irradiation. Journal of Photochemistry and Photobiology A: Chemistry, 329: 61-68. doi: 10.1016/j.jphotochem.2016.06.019.

Sarin, P., Snoeyink, V.L., Bebee, J., Jim, K.K., Beckett, M.A., Kriven, W.M. and Clement, J.A. 2004. Iron release from corroded iron pipes in drinking water distribution systems. Water Res., 38(5): 1259-1269. doi:10.1016/j.watres.2003.11.022.

Seliem, M. K., Komarneni, S. and Abukhadra, M. R. 2016. Phosphate removal from solution by composite of MCM-41 silica with rice husk: kinetic and equilibrium studies. Microporous and Mesoporous Materials, 224: 51-57. https://doi.org/10.1016/j.micromeso.2015.11.011

Sprynskyy, M., Buszewski, B., Terzyk, A.P. and Namiesnik, J. 2006. Study of the selection mechanism of heavy metal ($Pb^{2+}$, $Cu^{2+}$, $Ni^{2+}$, and $Cd^{2+}$) adsorption on clinoptilolite. J. Colloid Interface Sci., 304: 21-28. doi.org/10.1016/j.jcis.2006.07.068.

Takeda, A. 2003. Manganese action in brain function. Brain. Res. Rev., 41: 79-87. doi: 10.1016/S0165-0173(02)00234-5.

Tirtom, V.N., Dinçer, A., Becerik, S., Aydemir, T. and Çelik, A. 2012. Removal of lead (II) ions from aqueous solution by using crosslinked chitosan-clay beads. Desalination and Water Treatment, 39(1-3): 76-82.http://dx.doi.org/10.1080/19443994.2012.669161.

Tsai, W.C, de Luna, M.D.G., Bermillo-Arriesgado, H.LP. Futalan, C.M., James I. Colades, J.I. and Wan, M.W. 2016. Competitive fixed-bed adsorption of Pb (II), Cu (II), and Ni (II) from aqueous solution using chitosan-coated bentonite. International Journal of Polymer Science, 1-11. http://dx.doi.org/10.1155/2016/1608939.

Wang, G., Zhang, S., Wang, J., Ma, S., Lu, X. and Komarneni, S. 2016. Synthesis of porous Al pillared montmorillonite after preintercalation with dodecylamine: textural and thermal properties. Journal of Porous Materials, 23(6): 1687-1694. doi: 10.1007/s10934-016-0276-y.

Yang, M., Liu, X., Qi, Y., Sun, W. and Men, Y. 2017. Preparation of-carrageenan/graphene oxide gel beads and their efficient adsorption for methylene blue. Journal of Colloid and Interface Science, 506: 669-677. doi.org/10.1016/j.jcis.2017.07.093.

Zhang, Y., Li, J. and Li, W. 2015. Effect of particle size on removal of sunset yellow from aqueous solution by chitosan modified diatomite in a fixed bed column. RSC Adv., 5: 85673-85681. doi: 10.1039/c5ra13645h.

Zhua, H., Jiang, R., Xiao, L., Chang, Y., Guan, Y., Li, X. and Zeng, G. 2009. Photocatalytic decolorization and degradation of Congo Red on innovative crosslinked chitosan/nano-CdS composite catalyst under visible light irradiation. Journal of Hazardous Materials, 169(1-3): 933-40. doi: 10.1016/j.jhazmat.2009.04.037.